CrossMark

A New 2D Framework Based on 2,3′-Bipyridine-2′,3-dicarboxylate Copper(II) Units: Synthesis, Structure and Photoluminescence Properties
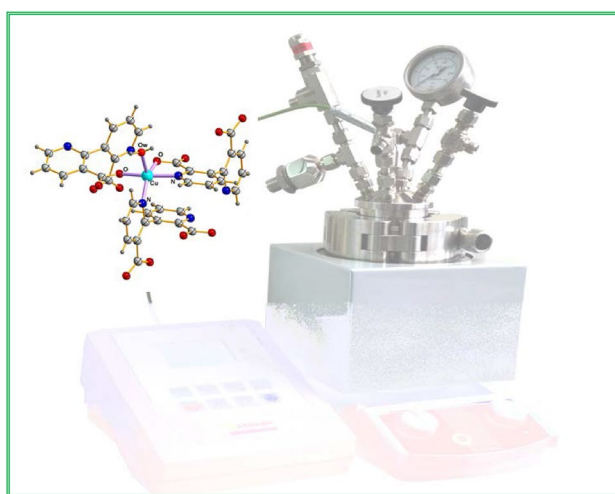
Kamil Twaróg[1] · Małgorzata Hołyńska[2] · Andrzej Kochel[1]

Abstract

A new ligand 2,3′-bipyridine-2′,3-dicarboxylic acid monohydrate (1) and a new copper(II) 2D coordination polymer [Cu(2,3′-2′,3-bpdc)H$_2$O]$_n$ (2) (2,3′-2′,3-bpdc = deprotonated bipyridinedicarboxylic acid) were synthesized and characterized by X-ray diffraction studies, IR spectra, elemental analysis, EPR, luminescence spectra and TGA. Magnetic properties measurements show weak antiferromagnetic coupling of the metal ions in the copper compound. These interactions are most likely assisted by hydrogen bonds.

Graphical Abstract

✉ Małgorzata Hołyńska
  holynska@chemie.uni-marburg.de

✉ Andrzej Kochel
  andrzej.kochel@chem.uni.wroc.pl

Extended author information available on the last page of the article

1 Introduction

Aminocarboxyl ligands can act as precursors of metal coordination polymers. Coordination polymers (CPs) are a thriving class of functional solid-state materials that have attracted much attention due to their potential use in various key applications, among them storage/separation, catalysis, molecular magnetism and non-linear optics [1].

In our previous work we described a 2D coordination polymer with aminocarboxylate 3,3′-bipyridine-2,2′-dicarboxylate (3,3′-bpdc) ligand, [Mn(3,3′-bpdc)]$_n$ [2]. Two new coordination polymers employing 2,2′-bipyridine-3,3′,6,6′-tetracarboxylate (bptc) as a ligand were also presented: [Mn$_2$(H$_2$O)$_5$(bptc)]$_n$ is a 2D coordination polymer stabilized by Mn−O coordination bonds, where magnetic interactions are transmitted within carboxylate bridged chains showing weak antiferromagnetic interactions and [Cu$_2$(H$_2$O)$_2$(bptc)]$_n$·2nH$_2$O forms polymeric double chains [3].

Sanram et al. obtained a series of Cu(II) MOFs using 1,4-phenylenedipropionic acid and different N,N′-donor coligands, namely, [Cu(ppa)(bpy)]$_n$ (**1**), {[Cu(ppa)(azp)(H$_2$O)](H$_2$O)}$_n$ (**2**), (H$_2$ppa = 1,4-phenylenedipropionic acid, bpy = 4,4′-bipyridine, azp = 4,4′-azobipyridine). The compound **4** is transformed from compound **3** by heating, through single-crystal-to-single-crystal transformation, adopting a CdSO$_4$-like (*cds*) 3D framework. All products were characterized with respect to their photocatalytic properties [4].

Other researchers used Cu(NO$_3$)$_2$·3H$_2$O as a substrate in hydrothermal syntheses to obtain MOFs with polycatenation and polythreading leading to 2D square grids [Cu(II)$_2$(5-HIPA)$_2$(4,4′-bipy)$_2$(H$_2$O)$_2$]$_n$ (**A**, 5-HIPA = 5-hydroxyisophthalato) and irregular layers [Cu(II)$_3$(5-HIPA)$_2$(2-PyC)$_2$(4,4′-bipy)$_2$(H$_2$O)$_4$]$_n$ (**B**) in a unique 3D framework [(**A**)(**B**)]·6.5nH$_2$O (**1**) with the in situ generated pyridine-2-carboxylate (2-PyC) ligand [5].

In 2014 Sasmal et al. obtained two Cu(II) coordination polymers {[Cu(HPymat)(MeOH)](NO$_3$)}$_n$ (**1**) and {[Cu$_4$(Pymab)$_4$(H$_2$O)$_4$](NO$_3$)$_4$} (**2**). Schiff-base ligands HPymat$^−$ and Pymab$^−$ [H$_2$Pymat = (*E*)-2-(1-(pyridin-2-yl)methyleneamino)terephthalic acid, HPymab = (*E*)-2-((pyridine-2-yl)methyleneamino)benzoic acid] were used as substrates. The compound **1** shows tetragonal EPR spectra in DMSO and DMF and inverse EPR spectrum in CH$_3$CN. The complex (**2**) shows rhombic EPR spectra in solid state at RT and 77 K and tetragonal spectra in DMSO, DMF and CH$_3$CN [6].

In Table 1 these compounds are classified with respect to ligand type and ligand coordination modes. The title copper(II) compound belongs to 2D frameworks with N,O-donor ligands.

Thus in this paper a new 2D coordination polymer is introduced, showing an interesting coordination mode for pyridine carboxylate ligand. Both ligand and the corresponding polymer are photoluminescent.

2 Experimental Section

2.1 General

Double-distilled water was used and Cu(BF$_4$)$_2$·H$_2$O was purchased and used as received.

2.2 Synthesis

2.2.1 2,3′-Bipyridine-2′,3-dicarboxylic Acid Monohydrate (1)

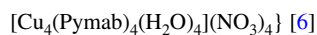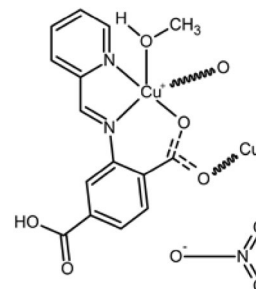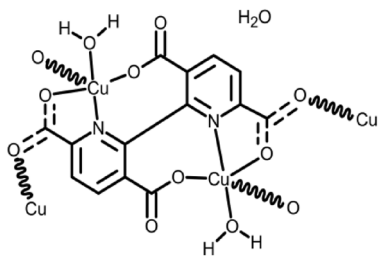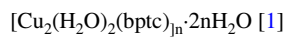A 100 cm^3 round-bottom flask was equipped with a reflux condenser and filled with 60 cm^3 of water. 1.00 g (0.180 mmol) of 1,7-phenanthroline and 0.4032 g (0.100 mmol) NaOH were added. The mixture was stirred for 15 min. Subsequently, 1.3941 g (0.876 mmol) of KMnO$_4$ was added in small portions and rinsing the corresponding weighing vessel with additional 10 cm^3 of water. The mixture was heated in oil bath and stirred at 95–97 °C for 10 h. The obtained solution was filtered from the MnO$_2$ side-product. Then active carbon was added and the suspension was heated at 95–97 °C for about 1 h. The mixture was filtered and left for cooling. The pH of the cool solution was adjusted to 3–4 by addition of 3M HCl dropwise. The obtained solution was left at room temperature for slow evaporation. After 2 days crystals in form of large plates suitable for X-ray diffraction studies were formed at 65% yield. The photographs with the single crystals of **1** are added in Fig. S6 in the Supplementary Material.

2.2.2 [Cu(2,3′-2′,3-bpdc)H$_2$O]$_n$ (2)

0.100 g (0.381 mmol) of (**1**), 10 ml of water and Cu(BF$_4$)$_2$·H$_2$O of (0.06 g, 0.234 mmol) were combined and sealed in a steel Teflon-lined Berghoff 100 autoclave. The use of stainless steel Berghoff autoclave allows for a one-pot synthesis of pure crystalline magnetic materials. Control of pressure (up to 100 bar) and temperature (up to 300 °C) in this setup ensures stable synthesis conditions and its reproducibility. The use of organic ligands narrows the synthesis temperature range to typically 100–300 °C, based on melting and decomposition points. The reagents are added in a Teflon insert. An advantage of solvothermal synthesis is the possibility to use reagents and solvents in which they are insoluble under normal conditions—for instance this advantage can be used to obtain (NH$_4$)$_2$[Re(NCS)$_6$]·4(CH$_3$)$_2$SO$_2$ product from dimethyl sulphone [7]. Organic solvents, such as alcohols and acetonitrile, are widely used but at limited scale due to safety

Table 1 Different types of metal–organic frameworks with N, O-donor ligands and various dimensionality

N, O-donor atoms in one ligand

[Cu$_2$(H$_2$O)$_2$(bptc)]$_n$·2nH$_2$O [1]
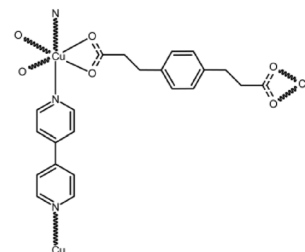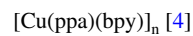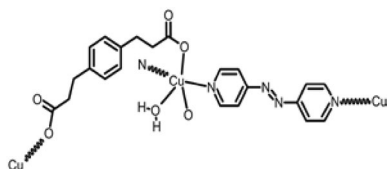
{[Cu(HPymat)(MeOH)](NO$_3$)}$_n$ [6]

[Cu$_4$(Pymab)$_4$(H$_2$O)$_4$](NO$_3$)$_4$} [6]

N, O-donor atoms in separate ligands

{[Cu(ppa)(azp)(H$_2$O)](H$_2$O)}$_n$ [4]

[Cu(ppa)(bpy)]$_n$ [4]
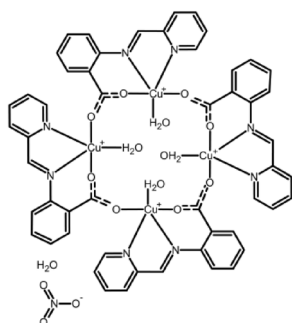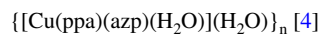
Table 1 (continued)

N, O-donor atoms in separate ligands

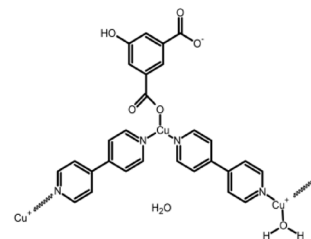[Cu(II)$_3$(5-HIPA)$_2$(2-PyC)$_2$(4,4′-bipy)$_2$(H$_2$O)$_4$]$_n$ [5]

[Cu(II)$_2$(5-HIPA)$_2$(4,4′-bipy)$_2$(H$_2$O)$_2$]$_n$ [5]
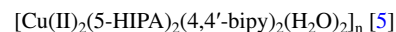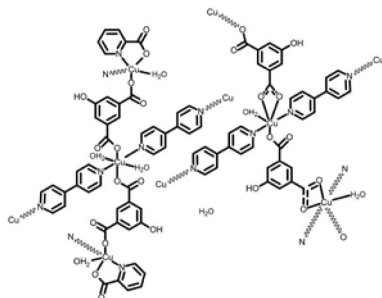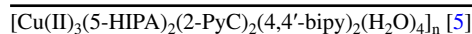
issues. After the synthesis the reaction mixture cools down very slowly which promotes crystallization of the product.

The mixture was heated at 135 °C for 5 days and subsequently slowly cooled down at 8 °C/h within 24 h. The resulting product comprised crystalline material with single crystals in form of blue prisms at 45% yield (estimated with respect to the 2,3′-bipyridine-2′,3-dicarboxylic acid monohydrate reagent for the crystalline products directly crystallized from the reaction mixture). The pictures with the single crystals of **2** are added in Fig. S7 in the Supplementary Material.

2.3 Characterization

2.3.1 IR Spectroscopy

2.3.1.1 IR Spectra were recorded with Bruker VERTEX 70 FTIR spectrometer for **1** and **2**. Selected bands from IR and spectra are presented as Supplementary Data S1, S2, Figs. S1a, b, S2a, b.

2.3.2 Elemental Analyses

2.3.2.1 CHN Elemental 1: Obs (Calcd for) %C 54.01 (54.96), %H 4.05 (4.40), %N 10.55 (10.68); **2** Obs (Calcd for): %C 44.23 (44.51), %H 2.51 (2.66), %N 8.43 (8.65).

2.3.3 Thermogravimetric Analyses

2.3.3.1 TGA Measurements were carried out on a SETARAM SetSys 16/18 TG-DTA device under nitrogen atmosphere with scanning rate at 10 K/min. for samples of **1** (13.63 mg) and **2** (6.15 mg) in the temperature range 40–1200 °C (see Supplementary Fig. S4 for **1**, Fig. S5 for **2**).

2.3.4 X-ray Diffraction Studies and Details of the Structures Refinement

2.3.4.1 X-ray Diffraction X-ray diffraction data for monocrystals of **1** and **2** were collected on an Xcalibur Ruby and KM4CCD Sapphire diffractometer [8] with MoK$_\alpha$ radiation at 100(2) K. Selected X-ray data are shown in Tables S1–S4 for **1** and **2** (ESI). CCDC reference numbers for **1** and **2**: CCDC 1543112 (**1**) and 1547821 (**2**) (Supplementary Data available from CCDC, 12 Union Road, Cambridge CB2, 1EZ, UK on request).

2.3.4.2 Crystal Structures Refinement The crystal structures were solved with direct methods in SHELXTL and refined using the full-matrix method in SHELXL [9]. Water/hydroxyl H atoms positions were initially refined with DFIX restraints (the O–H bond lengths at 0.84 Å and with $U_{eq} = 1.5U_{eq}$ (parent atom). Then these H atoms parameters were constrained. H atoms bonded to aromatic C atoms were generated using HFIX instuction with $U_{eq} = 1.2 - 1.5U_{eq}$ (parent C atom). Basic crystallographic data and selected bond lengths and bond angles are presented in the Supplementary Tables S2–S4.

2.3.5 EPR Spectra

EPR spectra were recorded at 77 K on a Bruker ELEXSYS E 500 CW-EPR spectrometer operating at X-band frequency and equipped with an ER 036TM NMR Teslameter and E 41 FC frequency counter. Spectra were measured at microwave power of 10 mW, modulation amplitude of 10 G and time constant 40 ms. The experimental spectra were simulated using the Bruker Win EPR SimFonia program, version 1.26 [10].

2.3.6 Photoluminescence Spectra

The photoluminescence spectra of **1** and **2** for solid crystalline samples anchored to quartz tubes were recorded with an FSL 980 Spectrometer from Edinburgh Instrument equipped with a 450 W Xenon arc lamp as an excitation source.

2.3.7 Studies of the Magnetic Properties

2.3.7.1 Magnetic Properties Magnetic susceptibility data were recorded on a Quantum Design MPMS-XL5 SQUID magnetometer over the 300–1.8 K temperature range. Magnetic data were corrected for diamagnetic contributions which were estimated from the Pascal's constants [11] and for temperature-independent paramagnetism estimated at 60×10^{-6} emu/mol for the Cu^{2+} ion [12].

2.3.8 NMR Spectra

NMR spectra were recorded on Bruker 500 MHz device.

For **1** see Supplementary Fig. S1 (^1H NMR spectrum, 500 MHz, D_2O, 300 K), Fig. S2 (^{13}C NMR spectrum, 125 MHz, D_2O, 300 K), Fig. S3 (2D spectra ^1H-^1H COSY, 500 MHz, D_2O, 300 K).

3 Results and Discussion

3.1 Syntheses

The synthesis of the ligand is illustrated in Scheme 1. $KMnO_4$ was used as an oxidizer and the MnO_2 side-product was filtered off from the reaction mixture. The amount of oxidizer was optimized to result in the highest yield. It should be emphasized that too high excess of the oxidizer may lead to further oxidation of the product. Scheme 1 summarizes the ligand synthesis (Schemes 1, 2).

2 is obtained in solvothermal syntheses from the following systems under hydrothermal conditions in the Berghoff autoclave.

The product was isolated in the pure crystalline form. Coordination modes displayed by the ligand are shown in the Scheme 3.

3.2 Analysis of the Crystal Structures

3.2.1 2,3′-Bipyridine-2′,3-dicarboxylic Acid (1) Crystal Structure Determination

2,3′-Bipyridine-2′,3-dicarboxylic acid (**1**) molecule comprises two pyridyl rings with N atoms at 2,3′ positions and
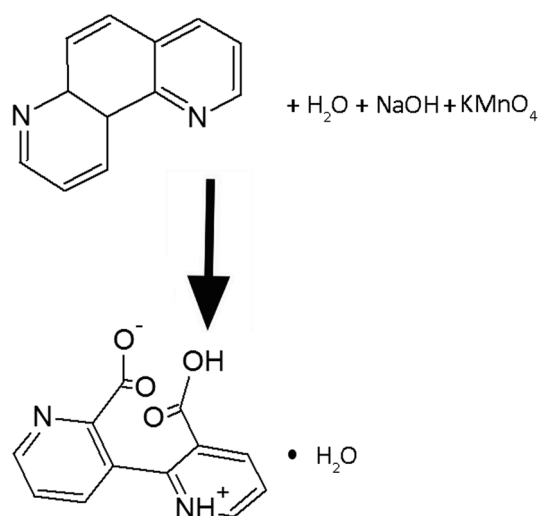
Scheme 1 Synthesis of the ligand (2,3′-2′,3-bpdc)·H_2O

two carboxylic groups substituting each of the aromatic rings. Molecular structure is shown in Fig. 1.

The torsion angle C5–C11–C10–C6 is of 72.60(17)° and describes the relative orientation of the carboxylic groups. The molecule adopts a zwitterion form with protonated N atom and de-protonated carboxylic group. Such zwitterionic form was also observed for 2,2′-bipyridine-4-methyl-3,3′-dicarboxylic acid monohydrate [13] and for rac-4,4′-bipyridine-2,2′-dicarboxylic acid monohydrate [14]. All of these zwitterionic compounds were isolated from aqueous solutions with neutral pH. The crystal structure of **1** is stabilized by a 3D hydrogen bonding network. The parameters of the corresponding hydrogen bonds are listed in Supplementary Table S5.

Extended hydrogen bonding network includes such graph set motifs as D_3^3 (12), D_3^3 (18), R_4^4 (14). Figure 2 illustrates one of such motifs.

3.2.2 2D Coordination Polymer Framework [Cu(2,3′-2′,3-bpdc)H₂O]ₙ (2)

The coordination polymer **2**, similarly as the ligand **1**, crystallizes in monoclinic space group type P2$_1$/c (basic crystallographic data are summarized in the Supplementary Material). In the asymmetric unit of the unit cell one ligand molecule is coordinated to the Cu^{2+} ion. In the coordination sphere also a terminal water molecule is present (Fig. 3).

The coordination number of the Cu^{2+} ion in **2** is 5. The coordination sphere is filled with 3 ligands: one is coordinated through N and carboxyl O atoms, the second ligand—through pyridine N atom and the third ligand through carboxyl O atom. The fifth coordination place is filled with the terminal water molecule (see Fig. 4).
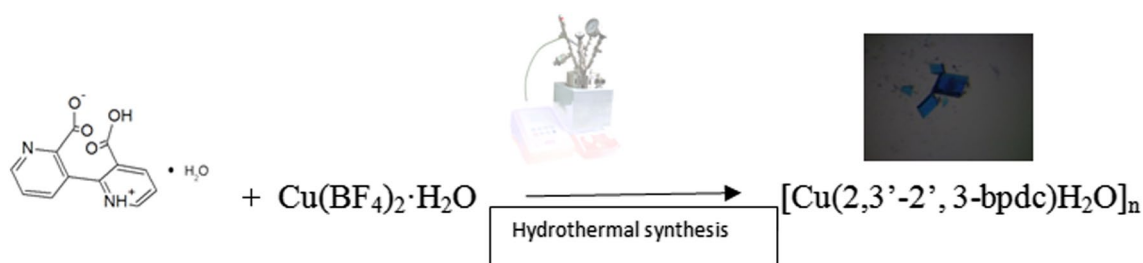
Scheme 2 Hydrothermal synthesis of [Cu(2,3′-2′,3-bpdc)H$_2$O]$_n$ (**2**)
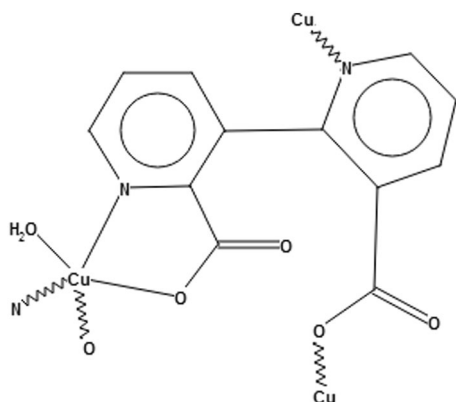
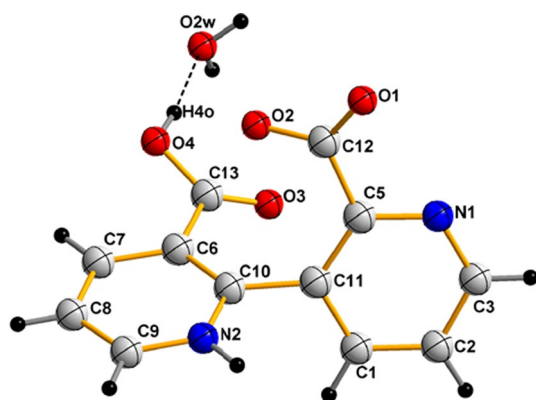**Scheme 3** Coordination modes displayed by the ligand in the compound **2**

Fig. 1 Molecular structure of **1**. Hydrogen bonding is denoted with a dashed line

The corresponding bond lengths are Cu1–O1 1.985(3), Cu1–N1 1.999(4), Cu1–O1w 2.180(3) Å and Cu1–O3 (− x + 1,y − 0.5, − z + 0.5) 1.933(3), Cu1–N2 (− x + 1, − y, − z + 1) 2.059(4). Similar bond lengths for terminal water ligand coordinated to a Cu^{2+} ion were also determined by Li-Yang Zhang et al. for a 2D coordination

polymer [Cu^{II}Cu$^{I}_2$(HPIDC)$_2$(H$_2$O)]$_n$ in which the Cu–H$_2$O bond length is of 2.2200(16) Å [15].

Also for another coordination polymer, [Cu(6-mepic)$_2$(H$_2$O)]·H$_2$O, the Cu–H$_2$O bond length is of 2.156(2) Å and thus is similar as in **2** [16]. The Cu–O bond lengths are of 1.96–2.15 Å and the Cu–N bond lengths are of 2.01–2.03 Å. The Addison τ parameter defined as $\tau = (\beta - \alpha)/60$ for α O3–Cu1–O1 85.69(18) and β O1–Cu1–N2 149.17(15) is 1.058, thus the coordination sphere is trigonal bipyramidal [17].

In the crystal structure hydrogen bonds of the O–H···O type are present. They not only stabilize the crystal structure but also might assist in transmission of magnetic exchange interactions (e.g. O2···H2w–O1–H1w···O4) [18, 19]. Additionally the hydrogen bonds link the 2D coordination polymer layers to form a 3D network (Fig. 5). The parameters of the corresponding hydrogen bonds are listed in Supplementary Table S6.

3.3 Other Properties

1 and **2** were characterized with a number of methods (see Experimental for elemental analyses and IR bands assignment). Also thermal decomposition under nitrogen atmosphere and the magnetic properties of **2** were investigated.

3.3.1 Thermal Decomposition

The thermal decomposition for both compounds was investigated at 40–1200 °C temperature range under nitrogen atmosphere (Supplementary pages 5 and 11). Experimental TGA data are presented in the Supplementary Material (Figs. S4 and S5). For the ligand **1** a 4-step decomposition process is observed. The first endothermal step at 190 °C involves evolution of water molecules (exp. 6.40%, calc. 6.86%). The second endothermal step is observed at 400 °C and may involve decarboxylation (exp. 10.84%, calc. 12.39%). The third peak at 600 °C most probably involves further degradation of the ligand organic part. The last exothermal peak at 900 °C (exp 11.43%) involves decomposition of the remaining organic part.

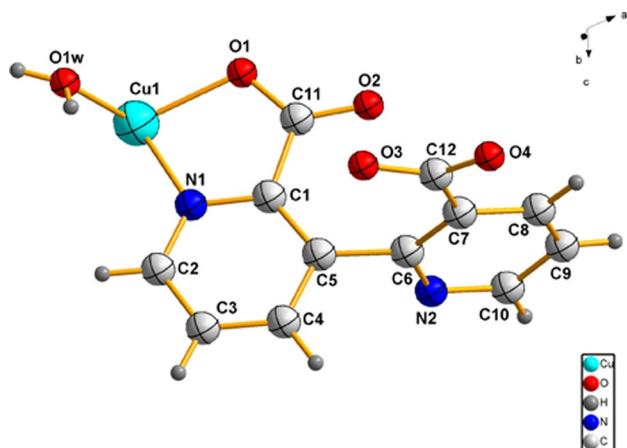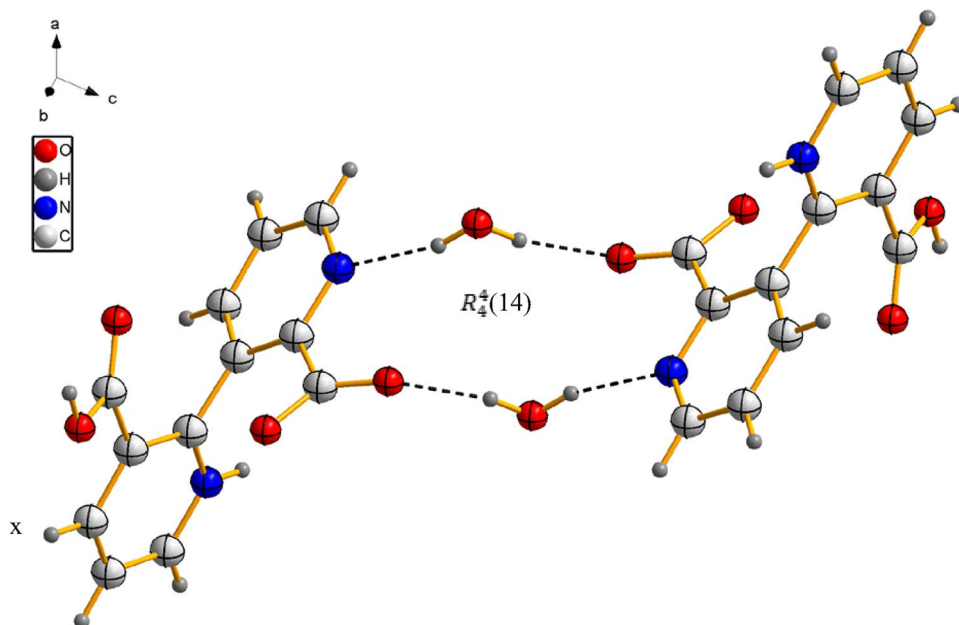**Fig. 2** One of the graph set motifs in **1**: R_4^4 (14). (Color figure online)

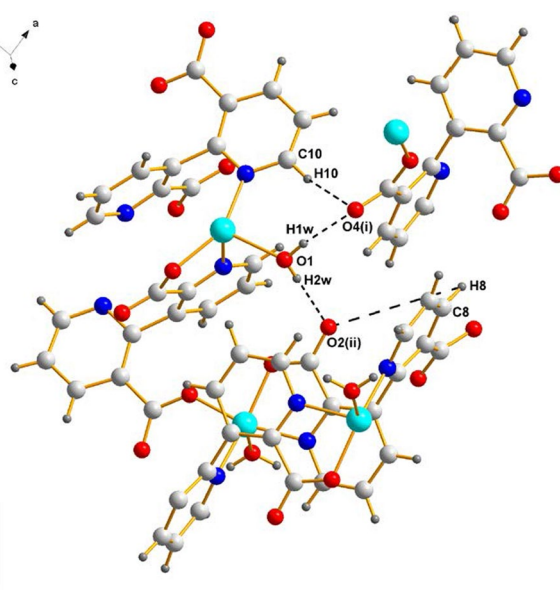**Fig. 3** Symmetry-independent part of **2**. (Color figure online)

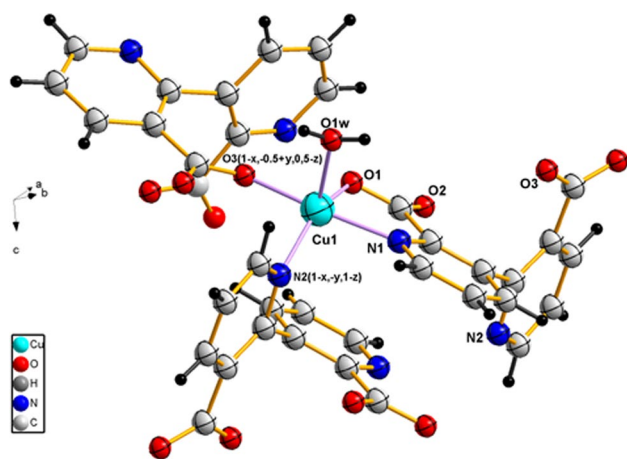**Fig. 4** Coordination sphere of the Cu^{2+} ion in **2**. (Color figure online)

Fig. 5 Hydrogen bonds system in the coordination polymer **2**. (Color figure online)

For the polymer **2** a 3-step decomposition process is observed. The first endothermal peak at 220 °C may correspond to the $C_{12}N_2O_2$ moiety (exp. 58.99%, calc. 61.01%). The second endothermal peak at 420 °C involves decarboxylation (exp. 21.39%, calc. 27.18%). The last exothermal peak at ca. 1000 °C should correspond to decomposition of the remaining part, leading to a mixture of Cu oxides as residue.
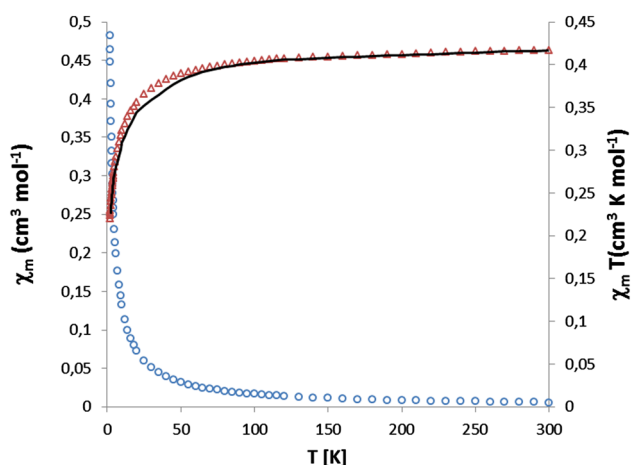
Fig. 6 Temperature dependence of the molar magnetic susceptibility χ_m (open circle) and the $\chi_m T$ product (triangle) for Cu **2** complex, calculated per one Cu(II) center. Solid lines are calculated curves with parameters presented in the text

3.3.2 Magnetic Properties

Magnetic susceptibilities of the complex **2** were measured in an applied magnetic field H = 0.5 T in the temperature range 1.8–300 K. As shown in Fig. 6 the $\chi_m T$ value at 300 K is of 0.416 cm^3 K mol^{-1} and decreases to 0.221 cm^3 K mol^{-1} at 1.8 K. In general, from 80 K the $\chi_m T$ values decrease which may correspond to antiferromagnetic interactions between the neighbouring Cu^{2+} ions in the coordination polymer. For measurements of the susceptibility data good fit to the Curie–Weiss law ($\chi_m = C/(T-\Theta)$) was achieved, giving Curie (C) and Weiss (Θ) constants of 0.58 cm^3 K mol^{-1} and −1.70 K, respectively.

The magnetic data for **2** were fitted using the magnetic chain model corresponding to the equation [20]:

$$\chi_m = \frac{N\beta^2 g^2 S(S+1)}{3kT} \frac{1+u}{1-u}$$

$$u = coth\left[\frac{JS(S+1)}{kT} - \frac{kT}{JS(S+1)}\right]$$

The best fit to the experimental data leads to the following values: J = −0.37 cm^{-1}, g = 2.15 and R = 2.97 × 10^{-5}. R is the agreement coefficient defined by the equation:

$$R = \sum_n^l (\chi_i^{exp} - \chi_i^{calc}T)^2/(\chi_i^{exp}T)^2$$

Temperature dependence of the molar magnetic susceptibility χ_m (○) and $\chi_m T$ are presented in Fig. 6. The closest interatomic Cu⋯Cu distances are 5.668(5) Å.

Analysis of the crystal structure leads to the conclusion that most probable magnetic interactions pathway is through hydrogen bonds involving water molecules: Cu1^i–O1^i–C11^i–O2^i⋯H2w–O1w–Cu1 (i = x, − 0.5 − y, − 0.5 + x).

The proposed pathway is illustrated in the Figure below, displaying the closest Cu⋯Cu distances (Fig. 7.).

Similar properties were observed by Decurtins et al. for 1D antiferromagnetic metal–organic framework [Cu(DCMB)(CA)]$_n$ where DCMB is 3.3′-dicarbomethoxy-2,2′-bipyridyl and CA is dianion of chloroanilic acid [21]. The exchange coupling constant (2J) value was estimated to be − 0.31 cm^{-1}.

In a different coordination polymer reported by Jan et al. {[Cu$_2$(bzgluO)$_2$(bpe)$_2$]·7H$_2$O}$_n$, where an N-donor ancillary ligand is H$_2$bzgluO = N-benzoyl-L-glutamic acid, bpe = 1,2-bis(4-pyridyl)ethane, the best fitting parameter obtained is J = − 0.85. The negative J value indicates that there is a weak antiferromagnetic interaction in the investigated complex [22].

Superexchange interactions through hydrogen bonds have been already observed in such copper(II) compounds as e.g. copper(II) complex, [Cu(LH)(L)]·BF$_4$·2H$_2$O (LH = N-tert-butyl-N-2-pyridylhydroxylamine)—in this case the magnetic interactions pathway was found to be Cu–O–H⋯O–Cu (Cu⋯Cu distance at 4.4669(12) Å) [23].

Other examples are [Cu(H$_2$O)(C$_7$H$_6$N$_2$)$_2$(C$_6$H$_6$O$_4$)] and isostructural [Cu(H$_2$O)(C$_7$H$_6$N$_2$)$_2$(C$_6$H$_8$O$_4$)] (C$_7$H$_6$N$_2$–benzimidazole, C$_6$H$_6$O$_4$-trans-2-butene-1,4-dicarboxylic acid) with antiferromagnetic interactions transmitted through a network of hydrogen bonds (Cu...Cu distances at 11.2383(6) and 10.926(1) Å, respectively) [24].

Gasque et al. used reaction between 2,8-dimethyl-5,11-bis(pyridine-2-ylmethyl)-1,4,5,6,7,10,11,12-octahydroimidazo[4,5-h]imidazo-[4,5-c] [1,6]-diazecine
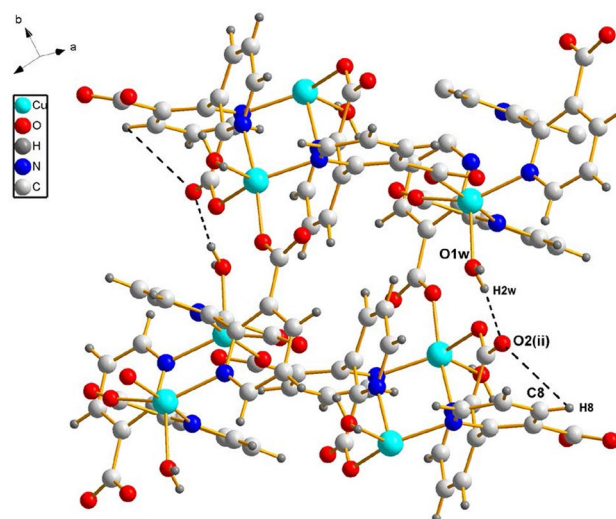

Fig. 7 Proposed pathway of the magnetic interactions in the studied coordination polymer (Cu–COO⋯H$_2$O⋯H$_2$O–Cu). (Color figure online)

(dimp) with copper(II) nitrate in water to obtain $[Cu_2(dimp)(H_2O)_2(NO_3)_2](NO_3)_2$ complex, also appearing to be the case of magnetic interactions transmission through hydrogen bonds (Cu...Cu distance at 6.255(2) Å) [25].

3.3.3 EPR Spectra

Powder EPR spectrum of the compound **2** recorded at 77 K shows a broad asymmetric band with simulated tensor values of $g_\perp = 2.08$, $g_{||} = 2.21$ (see Fig. 8). For coordination number 5 the possible border coordination geometries are trigonal bipyramidal (TBP) or square pyramidal (SP). The transition between them may occur as the energetic barrier is low for the ground state d_z^2, especially in solution [26, 27].

Broadening and extension of the spectrum is caused by interactions with the ^{14}N nuclei. The fact that $g_{||} > 2.1 > g_\perp > 2.0$ is connected with the distorted trigonal bipyramidal coordination environment of the Cu^{2+} ion (D_{3h}).

The obtained g values are characteristic for the related metal complexes with chromophore N_2O_2 groups. M. Padmanabhan et al. obtained the coordination polymer $[Cu(ipt)(dap)H_2O]_n \cdot nH_2O$ with isophthalate (ipt) as bridging moieties and chelating ligand 1,3-diaminopropane (dap) with similar Cu^{2+} coordination environment as in **2** for which $g_{||} = 2.158$ and $g_\perp = 2.074$ values were observed [28]. Higher $g_\perp > 2.04$ values are detected for the majority

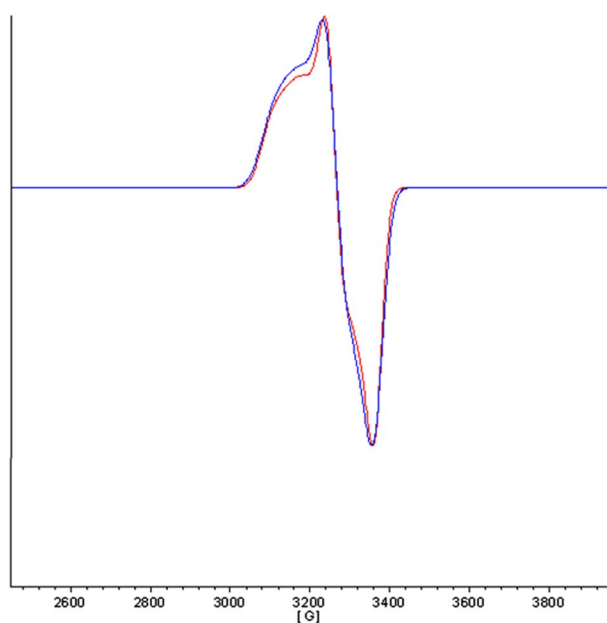of complexes with metal coordination environment of distorted trigonal bipyramidal symmetry [29].

3.3.4 Photoluminescence Spectra

The luminescent properties of **1** and **2** were explored in the solid state at room temperature (see Fig. 9). For the free ligand one emission band is observed with maxima at 385 and 401 nm. A band is formed by two constituents overlapping which can be assigned to charge-transfer and $\pi \cdots \pi^*$ transitions, respectively. For the coordination polymer **2** an emission band with a maximum at 482 nm is connected with blue–green emission (475–580 nm) attributed to ligand-to-metal charge transfer (LMCT) transition between the delocalized π electron density of the ligand and Cu(II) d orbitals. As a result, the emission can be assigned to the chelation of the carboxylate and bpy ligands to the central ions.

Transition metal complexes with the related ligands were considered for applications in organic light-emitting diodes (OLEDs) [30]. It could be expected that targeted modification of the compound **2** could improve its luminescence properties.

Similar spectra were recorded by Ji et al. for the {[Cu (bptc)$_{0.5}$(H$_2$O)]·H$_2$O}$_n$ coordination polymer with bptcH$_4$ ligand (bptcH$_4$ = 2,2′-bipyridine-3,3′,6,6′-tetracarboxylic acid) [31]. For the Cd(II) and Zn(II) coordination polymers with polypyridyl ligand the emission bands were found at 440–540 nm [32–35]. Yan-Zhi Tang et al. carried out hydrothermal syntheses using 2,2′-bipyridine-3,3′-dicarboxylic acid ligand to detect fluorescent emission fort the coordination polymer {[Cu(BDCD)]·EtOH}$_n$ where BDCB is anion of 2,2′-bipyridine-3,3′-dicarboxylic acid-1,1′-dioxide [36].

Fig. 8 Powder EPR spectra of the compound **2** at 77 K, the red line is the theoretical one. (Color figure online)
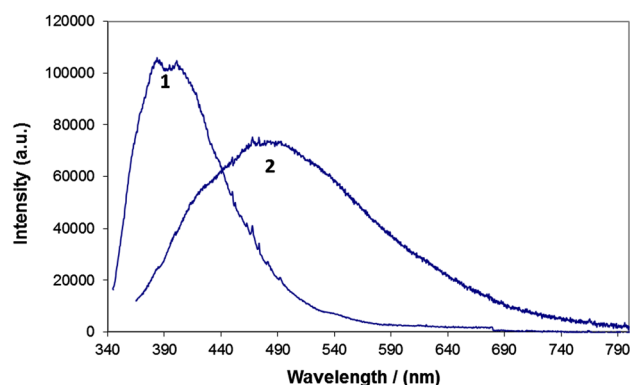

Fig. 9 Photoluminescence emission spectra excited with 385 nm (*1*) and 401 nm (*2*) of the ligand **1** and the polymer **2** with 482 nm in solid state at 297 K

4 Conclusions

A new ligand 2,3′-bipyridine-2′,3-dicarboxylic acid monohydrate (**1**) and its copper(II) 2D coordination polymer [Cu(2,3′-2′,3-bpdc)H$_2$O]$_n$ (**2**) were synthesized. Both **1** and **2** show photoluminescent properties confirmed with the corresponding emission spectra. For **2** the antiferromagnetic interactions between the Cu^{2+} ions may be transmitted also through hydrogen bonds. Based on this work the use of a Berghoff autoclave for reproducible solvothermal syntheses is demonstrated. The use of well-designed ligands in this method may lead to more useful photoluminescent products.

References

1. S. Kitagawa, R. Kitaura, S.I. Noro, Angew. Chem., Int. Ed. **43**, 2334 (2004)
2. M. Hołyńska, J. Kołodziejczak, A. Kochel, Inorg. Chim. Acta **436**, 214 (2015)
3. A. Kochel, M. Hołyńska, Inorg. Chim. Acta **408**, 193 (2013)
4. S. Sanram, J. Boonmak, S. Youngme, Inorg. Chim. Acta **469**, 11 (2018)
5. X.-Y. Cao, Q.-P. Lin, Y.-Y. Qin, J. Zhang, Z.-J. Li, J.-K. Cheng, Y.-G. Yao, Cryst. Growth Des. **9**, 20 (2009)
6. A. Sasmal, E. Garribba, C. Rizzoli, S. Mitra, Inorg. Chem **53**, 6665 (2014)
7. A. Kochel, M. Hołyńska, Acta Crystallogr. **C67**, m137 (2011)
8. Agilent, *CrysAlis PRO* (Agilent Technologies Ltd, Yarnton, 2014)
9. G.M. Sheldrick, Crystal structure solution and refinement with SHELXT, SHELXL. Acta Crystallogr. **C71**, 3 (2016)
10. WINEPR *SimFonia Version 1.26, Copyright (1994–97)*, Bruker analytical GmbH
11. E. König, *Magnetic Properties of Coordination and Organometallic Transition Metal Compounds*. (Springer, Berlin, 1966)
12. M.S. Caceci, Anal. Chem. **61**, 2324 (1989)
13. M. Hołyńska, A. Filarowski, A. Kochel, K. Twaróg, J. Chem. Crystallogr. **45**, 363 (2015)
14. R. Custelcean, M.G. Gorbunova, Cryst. Eng. Commun. **7**, 297 (2005)
15. L.-Y. Zhang, L.-P. Lu, S.-S. Feng, Acta Crystallogr. **C72**, 652 (2016)
16. F. Gracia, J. Perles, F. Zamora, P. Amo-Ochoa, Inorg. Chim. Acta **453**, 574 (2016)
17. A.W. Addison, T.N. Rao, J. Reedijk, J. van Rijn, G.C. Verschoor, J. Chem. Soc. Dalton Trans. (1984). https://doi.org/10.1039/DT9840001349
18. S.I. Levchenkov, I.N. Shcherbakov, L.D. Popov, V.V. Lukov, V.V. Minin, Z.A. Starikova, E.V. Ivannikova, A.A. Tsaturyan, V.A. Kogan, Inorg. Chim. Acta **405**, 169 (2013)
19. Z. Vasková, J. Moncol, M. Korabik, J. Medvecká, J. Švorec, Z. Padelková, M. Valko, D. Valigura, Polyhedron **30**, 86 (2011)
20. O. Kahn, *Molecular Magnetism*. (VCH Publishers, New York, 1993)
21. S. Decurtins, H.W. Schmalle, L.-M. Zheng, J. Ensling, Inorg. Chim. Acta **244**, 165 (1996)
22. M.-J. Yan, Q. Feng, H.-H. Song, H.-T. Yu, Inorg. Chim. Acta **450**, 304 (2016)
23. A. Okazawa, T. Ishida, Chem. Phys. Lett. **480**, 198 (2009)
24. L. Sieroń, M. Bukowska-Strzyżewska, M. Korabik, J. Mroziński, Polyhedron **21**, 2479 (2002)
25. J. Sánchez Costa, N.A.G. Bandeira, B. Le Guennic, V. Robert, P. Gamez, G. Chastanet, L. Ortiz-Frade, L. Gasque, Inorg. Chem. **50**, 5696 (2011)
26. R. Barbucci, A. Bencini, D. Gatteschi, Inorg. Chem. **16**, 2117 (1997)
27. B.A. Bencini, D. Gatteschi, Inorg. Chem. **16**, 1994 (1977)
28. M. Padmanabhan, K.C. Joseph, A. Thirumurugan, X. Huang, T.J. Emge, J. Li, Inorg. Chim. Acta **360**, 2583 (2007)
29. B.J. Hathaway, D.E. Billing, Coord. Chem. Rev. **5**, 143 (1970)
30. H. Xu, R. Chen, Q. Sun, W. Lai, Q. Su, W. Huang, X. Liu, Chem. Soc. Rev. **43**, 3259 (2014)
31. B. Ji, D. Deng, X. He, X. Fan, G. Qu, Inorg. Chim. Acta **416**, 102 (2014)
32. C.-G. Zheng, Y.-L. Xie, R.-G. Xiong, X.-Z. You, Inorg. Chem. Commun. **4**, 405 (2001)
33. J. Zhang, Y.-R. Xie, Q. Ye, R.-G. Xiong, Z.-L. Xue, X.-Z. You, Eur. J. Inorg. Chem. **14**, 2572 (2003)
34. J.-H. Luo, M.-C. Hong, R.-H. Wang, R. Cao, L. Han, Z.-Z. Lin, Eur. J. Inorg. Chem. 2705 (2003)
35. L. Han, M.-C. Hong, R.-H. Wang, J.-H. Luo, Z.-Z. Lin, D.-Q. Yuan, Chem. Commun. 2580 (2003)
36. Y.Z. Tang, M. Zhou, H.-R. Wen, Z. Cao, X.-W. Wang, S. Huang, CrystEngComm **13**, 3040 (2011)

Affiliations

Kamil Twaróg[1] · Małgorzata Hołyńska[2] · Andrzej Kochel[1]

[1] Department of Chemistry, Wrocław University, F. Joliot Curie 14, 50 383 Wrocław, Poland

[2] Fachbereich Chemie and Wissenschaftliches Zentrum für Materialwissenschaften, Philipps-Universität Marburg, Hans-Meerwein-Straße, 35043 Marburg, Germany